Drag force on a spherical intruder in a granular bed at low Froude number

J. E. Hilton[1] and A. Tordesillas[2]

[1]*CSIRO Computational Informatics, Melbourne, Australia*
[2]*Department of Mathematics and Statistics, Melbourne University, Australia*

The drag force on an object, or "intruder," in a granular material arises from interparticle friction, as well as the cyclic creation and buckling of force chains within the material. In contrast to fluids, for which drag forces are well understood, there is no straightforward relationship between speed and mean drag force in granular materials. We investigate spherical intruder particles of varying radii moving at low speeds through granular beds. The system can be parametrized using the dimensionless Froude number $\mathrm{Fr} = 2v/\sqrt{gR}$, for intruders of radius R moving at a speed v. For frictional systems, we find the drag force obeys a linear relationship with Fr for low Froude numbers above $\mathrm{Fr} > 1$. For $\mathrm{Fr} < 1$ we observe a deviation from this linear trend. This transition can be explained by considering the characteristic inertial and gravitational granular time scales of the system. We show that a suitably normalized measure of dissipated power obeys a linear relationship with the imposed intruder velocity, independent of the intruder dimensions. This is found to hold even for particles with no friction, identifying a relationship between the imposed motion of the intruder and the resistance of the granular material to purely geometric rearrangements.

I. INTRODUCTION

In comparison to the well-known drag forces for objects immersed in fluids, the investigation of drag forces on objects in granular media is an active and relatively new research area. In part this is due to the complexity of granular material which, unlike fluids, do not have a fully encompassing macroscopic constitutive formulation. Instead, granular materials can be regarded as a network of contacts which not only exhibit complex dynamics as they evolve under load, but is also a medium through which complex and multiscale processes occur. From this perspective, forces on objects (commonly referred to as "intruders") in response to imposed motion can be viewed as a measure of resistance to structural rearrangement within the granular material. These forces act in addition to any interparticle frictional forces which may be present. Arguably the most striking aspect of drag or resistance to moving objects in granular beds is the emergence of two cojoined strong and weak particle networks [1–3]. Similar to architectural constructions, those in the strong network (the force chains) form columns in alignment with the major (most compressive) principal stress, while those in the complementary weak network form trusses which confine and laterally brace the force chains [1–5]. Rearrangements in the material are a result of the collapse of axially compressed force chains by buckling, along with the creation of new force chains which form at locally jammed sites within the bed [6]. Experiments by Geng and Behringer have shown that the coexisting creation and failure of these force chains constitutes the principal mechanism responsible for the drag force experienced by intruders in dense granular material [7,8]. This rearrangement can also clearly be seen if a single particle in the bed is gradually loaded until failure occurs [9]. If the load on an intruder within the bed is maintained, multiple cycles of buckling and reformation can occur. As the rearrangement time scale is typically much shorter than the time scale between failure events, these manifest as stick-slip cycles [10,11]. Consequently, fluctuations govern the instantaneous drag force

measured in a granular bed. However, a mean drag force can be found if these forces are averaged over many of these cycles. This drag force, which represents the macroscopic response of the bed, can therefore give some insight into the complex dynamics of force chain evolution occurring within the granular media.

Understanding the mechanism governing the forces acting on solid objects in granular materials is important in many real-world settings. These include the prediction of failure in soil-structure interaction [12,13], the characterization of stick-slip in laboratory faults in earthquake mechanics [14], the modeling of damage from large-scale geophysical events (e.g., avalanches [15–17] and landslides [18]), and the optimization analysis of a myriad number of industrial operations associated with the handling, transport, and processing of powders and grains [19]. The large length scales and grain numbers in such real-world systems make the granular mechanics giving rise to forces very difficult to identify in detail. In this study, we reduce the loading on a granular system to a single intruder. This allows a careful examination of the mechanism of response, which may be directly applicable to these larger systems.

Despite the considerable attention devoted to the study of force chains, the connection between these emergent load-bearing structures and granular drag has not yet been fully characterized. Moreover, the existing literature, covering the range of experimental and theoretical studies, has mainly focused on the two flow regimes at the opposite ends of the spectrum: quasistatic and dynamic. The intermediate or transition flow regime, wherein arguably the richest dynamics occur, remains largely unexplored. Our ultimate aim is to characterize this transition regime across the micro-meso-macro levels. To achieve this, we employ a two-stage approach. This first stage focuses on the connection between the drag force and the two known sources of granular strength at the microscopic (particle) level: interparticle friction and geometric impenetrability. The next stage, which will be reported in a future study, will focus on the connection

between the drag force and the mesoscopic structures of force chains within the system. We note that the limiting case of zero inter-particle friction is intimately tied to geometric impenetrability, the effects of which often manifest through Reynolds' dilatancy [20–22]. In order for the intruder to advance, the particles in the bed must be moved from the path of the intruder, leading to dilatancy. In other words, work must be done against any confining pressure to shear the granular bed.

The rest of this paper is arranged as follows. We devote the remaining subsections of this Introduction to a brief review of the extant literature on granular drag for the quasistatic and dynamic regimes, before a brief outline of our strategy to the characterization of the intermediate regime. We present the methodology in Sec. II, followed by our results in Sec. III. Finally, a summary of our findings and future research directions is given in Sec. IV.

A. Quasistatic regime

A number of studies have previously been carried out to investigate granular drag forces. In the quasistatic regime, the first to study the force on plates and cylinders drawn through a bed of granular material was Wieghardt [23], who found a force dependence of $h^{5/2}$, where h is the depth of the intruder below the free surface. The force on a number of different intruder shapes, including spheres, within in a granular bed has also been investigated in detail by Albert *et al.* [10,24,25]. Their experimental setup used a horizontal rotating granular bed into which a cylinder was vertically immersed, the force on which was recorded using a load cell. For determining the forces on differently shaped intruders, a thin cylinder was used with the intruder attached to the end. Typical intruder speeds studied in this "slow drag" regime were O(1 mm/s). The drag force was found to be a function of the cross-sectional area and a quadratic function of the intruder depth below the granular surface. The drag force in all cases was, however, found to be independent of the speed of the intruder. Such a relationship has also been found to hold for other shapes, such as vanes immersed in a granular medium [26]. This unintuitive finding results from the requirement that any externally imposed rearrangement of the the bed must involve the buckling of force chains. Unlike fluids, the drag force on an intruder in a granular material instantaneously jumps to a threshold value at nonzero speed. As pointed out by Albert *et al.* [10], this minimum force gives an insight into the local jamming and buckling mechanisms in granular materials. The forces on a horizontal, rather than vertical, cylindrical intruder moving at slow speeds have been investigated experimentally and computationally by Ding *et al.* [27]. Forces in their setup were also found to be independent of the speeds considered in their study, $v < 0.4$ m/s. A further finding was a net shape-dependent lift force on the intruder. Interestingly, their work is part of a wider study on the locomotion of a unique creature which executes an undulating motion that is a cross between a snake and a fish, thereby exploiting the solidlike and fluidlike properties of sand to generate propulsion [28]. Geng *et al.* have investigated the slow drag regime in a two-dimensional experimental setup, using a horizontally rotating annulus filled with disks [8]. The force on an intruder fixed relative to the flow of disks was measured using a load cell. This was found to slowly increase with rotation speed, rather than being effectively constant, as reported by Albert *et al.* [10].

B. Dynamic regime

Several studies have investigated the forces on intruders in the high-speed, dynamic regime. Here, the bed is fluidized in the wake of the intruder, forming a similar structure to a fluid bow shock wave [29,30]. In this dilute regime, the drag forces are dominated by momentum transfer from grains impacting on the intruder and the drag force follows the classical quadratic drag law of fluids [31]. Such studies are usually carried out in vertical chutes, or in simulations using jets of particles in which gravity is not considered [29,31]. Careful investigations of the forces on a cylinder in a rapid vertical stream of particles have revealed a transition from an effectively discrete to continuum system as the Knudsen number approaches unity [32]. This transition bears close similarity to transitions in supersonic gas flow around objects. Such systems are also of interest for high-speed impact and subsequent penetration of objects into granular beds [33]. Horizontal motion of a cylindrical intruder has recently been investigated [30], where a quadratic drag law was found to hold at high speeds and small intruder depths. Wake formation, similar to the vertical setup, was also observed independent of depth at high intruder speeds.

C. Characterization of the intermediate regime

Our strategy for the characterization of the intermediate regime is to simplify the load on a granular system to a single intruder, allowing us to develop an understanding of the basis for the forces resisting motion within a granular bed. In this study we consider a sphere moving horizontally through a packed bed of grains at speeds within the intermediate regime between the quasistatic and dynamic regimes. We chose a sphere, as it represents the simplest possible intruder shape and can be compared to similar drag systems in fluid mechanics, such as Stokes drag. Previous studies have investigated either experimental analogs, such as a rod drawn through a granular bed, or have restricted their investigations to two-dimensional systems [30]. This intermediate flow regime has received little attention, although it contains potentially the most interesting transition in granular dynamics for this system. The existence of a transition can be determined by considering two characteristic time scales for an intruder moving horizontally in a granular bed [24,30]. The first is the time for a particle to fall back into the bed as the intruder moves past, $\tau_p = 2\sqrt{R/g}$, where R is the intruder diameter and g gravitational acceleration. The second is the time scale of the intruder movement $\tau_i = R/v$, where v is the intruder speed. The transition between these time scales therefore occurs at $\tau_p/\tau_i = 1$, where this ratio is the Froude number for the system, $\mathrm{Fr} = 2v/\sqrt{gR}$. In this study we investigate the dynamics around a Froude number ∼1, as well as the dependence of the drag forces on the intergrain friction. The case with zero intergrain friction is also considered, where the drag forces can only result from the resistance to structural rearrangement in the bed. It should be noted that

a horizontally driven system, such as the one used in this study, is very different from a vertical system as used by, for example, Chehata *et al.* [34]. In a vertical system, the flow direction and gravity are aligned so there is no comparable τ_p and therefore no equivalent transition at Fr = 1 from the competition between gravitational stabilization of the bed and the forcing from the intruder particle.

II. METHODOLOGY

The setup consisted of a particle bed of dimensions 2×2 m in the x and z directions, respectively, filled to a height of 1.3 m in the y direction. A large spherical intruder, initially centered in the bed, was moved at a constant velocity along the x axis. This setup is shown schematically in Fig. 1. Gravitational acceleration was fixed in the vertical y direction at -9.8 m/s^2. The particles filling the bed were spheres of mean radius 25 mm, with a random $\pm 10\%$ variation in diameter to provide a polydisperse packing, preventing crystallization effects. Intruder radii of 50, 75, 100, and 125 mm were used. The total number of particles used was approximately 50 000. A number of different driving velocities were applied to the intruder, varying from 0.05 to 2.5 m/s. Any interstitial gas effects were neglected in this study, as it was assumed that they were negligible in comparison to the interparticle forces.

The system was computationally modeled using the discrete element method. Forces and torques on each particle in the system were individually summed from the interactions with only neighboring particles. This locality is allowable as the time step Δt in the system was set to be $\Delta t < r_{\min}/v_p$, where $r_{\min}$ is the smallest particle radius in the system and v_p is the elastic p-wave speed within the particles. This time step,
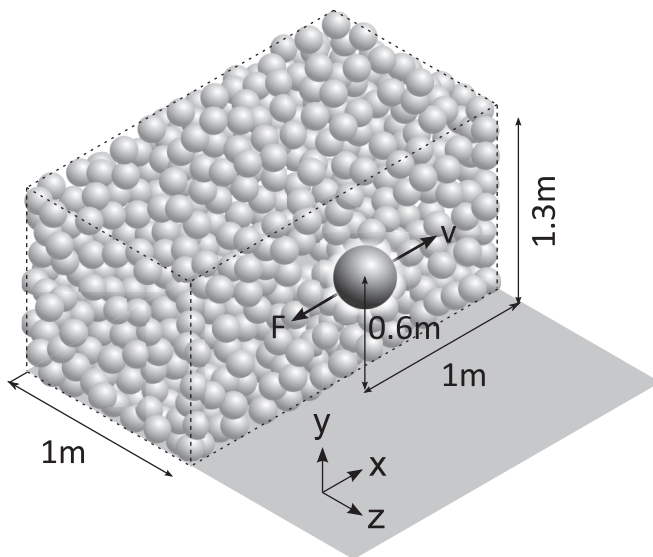

FIG. 1. Schematic cutaway of the setup used (not shown to scale). A large spherical intruder particle of radius R is moved through a bed of particles at an imposed speed along the x axis, 0.6 m above the base of the bed. The domain is 2×2 m in the x and z directions, respectively, with a free surface approximately 1.3 m above the base. Periodic boundary conditions are applied in the x and z directions. The lower boundary condition consists of a layer of fixed particles.

similar to the Courant-Friedrichs-Lewy condition for fluid dynamics, ensures that disturbances in the system could only propagate less than one particle radius during each time step. Once the forces and torques on each particle were determined, the system was integrated forward in time using a Verlet scheme to give the positions and velocities of the particles at the next time step.

We used the nonlinear Hertz-Mindlin contact model to calculate the normal and tangential forces at contact points between particles. Although this contact model is more computationally expensive than more commonly used contact models, such as linear Kelvin-Voigt formulations, it has a stronger physical basis as it uses a Hertzian contact force in the normal direction. The accuracy of the contact model is paramount in slow granular processes, such as the ones modeled for this study. Furthermore, it allows the use of physical constants in the simulation, such as Young's modulus and the Poisson ratio, without having to tune parameters to provide an approximation in the model for these constants.

In the Hertz-Mindlin model the contact force between two particles $\mathbf{F}_c$ is the vector sum of the normal contact forces $\mathbf{F}_n$ and the tangential contact forces $\mathbf{F}_t$, $\mathbf{F}_c = \mathbf{F}_n + \mathbf{F}_t$. The normal contact force is modeled using a Kelvin-Voigt model with a nonlinear spring,

$$\mathbf{F}_{ijn} = -\left(K_n \delta l_{ij}{}^{3/2} + C_n \mathbf{v}_{ijn} \cdot \mathbf{n}_{ij}\right)\mathbf{n}_{ij}, \tag{1}$$

for two particles with indexes i and j, where K_n is a spring stiffness, l_{ij} the particle overlap, $\mathbf{v}_{ij}$ the relative velocity vector, and $\mathbf{n}_{ij}$ the displacement vector between the centers of the two particles. The spring stiffness for particles of identical Young's modulus E and Poisson ratio ν is given by

$$K_n = \frac{2}{3} \frac{E\sqrt{r'}}{(1-\nu^2)}, \tag{2}$$

where r' is the effective particle radius given by $r' = r_i r_j/(r_i + r_j)$. The normal damping coefficient is calculated as

$$C_n = \alpha l_{ij}^{1/4}\sqrt{mK_n}\sqrt{\delta l_{ij}}, \tag{3}$$

where α is an empirically determined constant [35]. The tangential force is modeled using a Kelvin-Voigt formulation, incrementally calculated by

$$\mathbf{F}_t = \min\left[\tan(\theta)|\mathbf{F}_n|, \sum K_t \mathbf{v}_t \, \Delta t + C_t \mathbf{v}_t\right], \tag{4}$$

where θ is the friction angle, K_t the tangential spring stiffness, $\mathbf{v}_t$ the relative tangential velocity, Δt the incremental time step, and $C_t = C_n$ is a tangential damping coefficient. The friction angle is related to the coefficient of friction μ by $\mu = \tan(\theta)$. The static and dynamic friction coefficients are also assumed to be equal in these simulations. The incremental sum models the tangential elastic deformation of the surface, which is limited by the Coulomb friction $\mu|\mathbf{F}_n|$ acting in the direction opposing the applied force. The tangential spring stiffness K_t in the Hertz-Mindlin model is given by

$$K_t = \frac{2E\sqrt{r'}}{(1+\nu)(2-\nu)}\sqrt{\delta l_{ij}}. \tag{5}$$

The bed was filled by creating a set of nonoverlapping particles and allowing them to settle around the intruder under gravity. Periodic boundary conditions were imposed in the
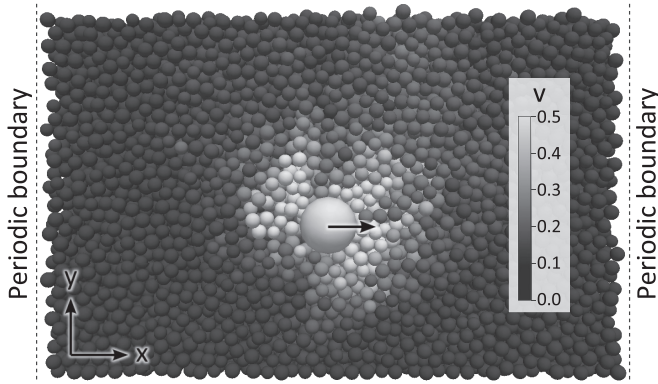
FIG. 2. Cross section of particle bed showing particles shaded by speed (m/s) at 4 s into a simulation. The large central intruder particle is 100 mm in radius and has an imposed velocity of 1 m/s along the x axis. All particles have a friction angle of $15°$. Periodic boundary conditions are applied in the x and z (not shown) directions.

x and z directions. This gave effectively "open" granular boundaries in the horizontal directions and allowed the intruder particle to repeatedly cycle through the bed at higher velocities. Fixed boundaries were not used, as these would cause the force chains to terminate prematurely as the intruder approached the boundary. Care was taken to ensure the periodic boundary conditions did not interfere with the dynamics of the system. Simulations at high velocities were inspected to ensure that the intruder always moved into a static region of the bed, and the repeated cycling through the periodic boundaries did not cause a net motion to accumulate over all the particles in the bed (this was found to occur for simulations in much smaller domains). The top boundary condition was a free surface, and the simulations were inspected to ensure that the intruder was at a sufficient depth for negligible surface deformation to occur. The lower boundary condition was a layer of frozen particles to ensure a rough fixed base of particles, representing a lower static bed. An example case of a 100-mm radius particle moving at 1 m/s is shown in Fig. 2, where particles are shaded by speed. The movement can be seen to be limited to the local area surrounding the particle, with static particles elsewhere in the bed.

We investigated the force dependence on friction and particle diameter at a range of velocities. As we were concerned with the low-Froude-number regime, a larger number of low-velocity than high-velocity cases were used. The dependence on depth has been studied in detail, and is known to be a quadratic function of intruder depth [24]. Due to this, the depth was not varied in this study and the center of the intruder was fixed in our investigation at 0.7 m below the mean free surface, and 0.6 m from the lower boundary. The parameters used in the simulations in this study are shown in Table I. The physical parameters used for the particles were chosen to represent the stiffest possible material that could be calculated in a tractable computational time. The values used gave an effective spring constant in the normal direction of $K_n \sim 1 \times 10^8$ kg/(s$^2\sqrt{\text{m}}$). All simulations used the open source software Yade for the discrete element calculations [36], as well as the measurement of the net force on the sphere. The software has been extensively validated for many types

TABLE I. Simulation parameters used.

Parameter	Symbol	Value
Young's modulus	E	1×10^9 Pa
Poisson ratio	ν	0.3
Coefficient of restitution		0.5
Density	ρ	2700 kg/m^3
Intruder depth		0.7 m
Intruder radii	R	$50, 75, 100, 125$ mm
Bed sphere radii	r	25 mm
Friction angles	θ	$0°, 7.5°, 15°, 30°$

of granular flow, ranging from quasistatic [37] to rapid flow conditions [15]. The supplied Hertz-Mindlin model was used to simulate the contact mechanics [38].

To measure the drag force, the x component of the force on the intruder was recorded. Drag forces in granular materials originate from cycles of stick-slip loading and unloading from microscale mechanics [24]. Due to this, any instantaneous forces measured are highly variable and must be averaged over many loading cycles to give a mean force. Here, we allowed the system 1 s to settle and calculated the subsequent cumulative average force in the x direction on the particle. An example force plot is shown in Fig. 3, with the cumulative average overlaid. It can be seen that although the instantaneous force rapidly fluctuates, the cumulative average quickly reaches a steady value. All simulations calculated the drag forces over 10 s in total, and the cumulative average from 1 to 10 s was taken as the average drag force on the intruder. The time steps in the simulations were O(10^{-5}) s.

III. RESULTS

The average nondimensionalized force in the x direction $\bar{F}$, measured on the intruder particle, is plotted against the intruder Froude number for friction angles of $15°$ and $30°$ in Fig. 4 and $0°$ in Fig. 5. The force was nondimensionalized by dividing by the average weight of a particle in the bed,
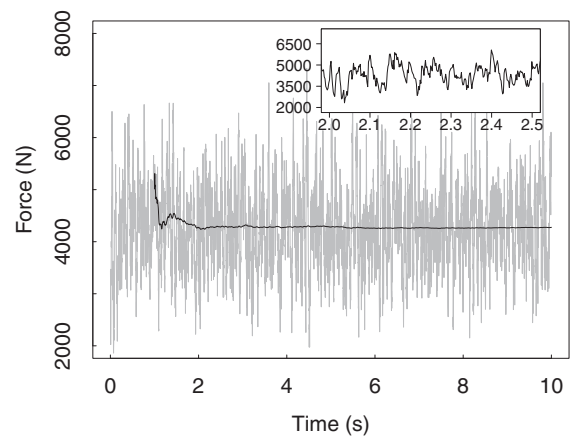

FIG. 3. Instantaneous force measured on an intruder particle 100 mm in diameter moving at 1 m/s (gray line) and cumulative average force from 1 s onwards (black line). The inset shows an example of multiple stick-slip cycles occurring in the instantaneous drag force from 2 to 2.5 s.
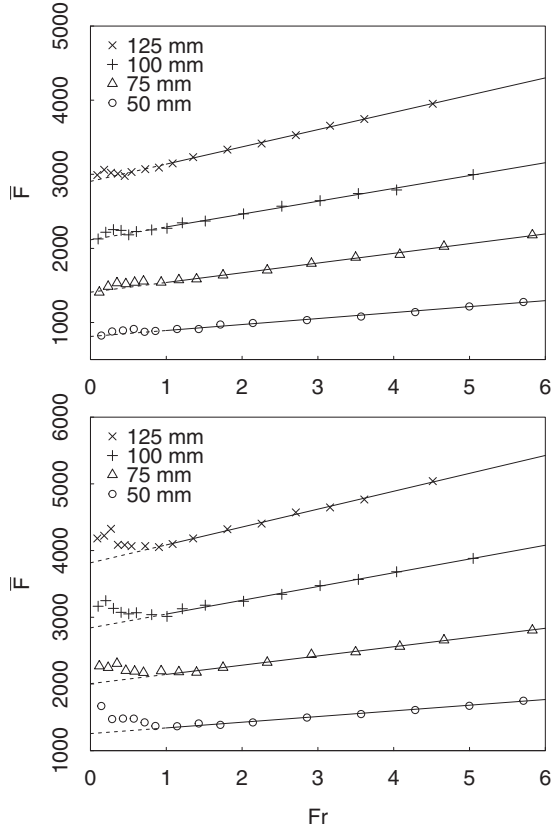
FIG. 4. Mean nondimensionalized force in x direction on intruder particle against intruder for a system with a friction angle of $15°$ (upper) and $30°$ (lower). The solid line is a best-fit spline. Four intruder particle radii are shown, $50, 75, 100,$ and 125 mm.

$\bar{F} = F/(4\pi\rho r^2)$, where F is the mean measured force, ρ the particle density, and r the average radius of the particles in the bed. In all cases, it was found that the drag force was nonzero as the Froude number approached zero. This effect has previously been investigated in detail [23,24,30] and, as previously discussed, results from the minimum force required
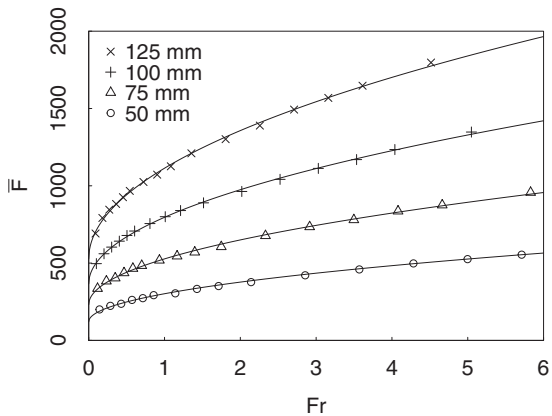

FIG. 5. Mean nondimensionalized force in x direction on intruder particle against Froude number for a system with a friction angle of $0°$. The solid line is a fit to a function of the form F $-$ const $\propto \sqrt{\text{Fr}}$. Four intruder particle radii are shown, 50, 75, 100, and 125 mm.

to buckle force chains, allowing rearrangement of the bed to occur.

In the cases with friction, the measured force flattens at low Froude numbers, giving a force that appears approximately constant at low velocities. The small upward turn in the trend at low Froude numbers for a friction angle of $30°$ is unexpected and may result from averaging the data at low speeds. However, a similar trend appears in a comparable experimental plot by Wieghardt [23] for intruders well below the granular surface. Further work is required to investigate this phenomenon in detail. Above a Froude number of Fr $\sim$ 1 the force follows a linear trend, which is plotted in Fig. 4 as a solid black line. This linear trend has been extended for visual comparison as a dashed line to Fr $= 0$. For all Fr > 1 this trend matches a linear model with $R^2 > 0.99$. Drag forces given by Geng and Behringer [8] follow a similar increase in force with respect to relative velocity in their two-dimensional setup. The drag forces reported by Potiguar and Ding [30] use a friction angle of approximately $15°$ and show comparable results for intruders immersed at half the depth of the granular bed. Although a quadratic dependence was found to fit well for intruders near the surface, they note evident deviation from a quadratic dependence for intruders deeply immersed within the bed. The available data from their study for the Froude range considered here (Fr < 6) appears to also match a linear trend.

The case with zero friction is markedly different from the cases with friction. In each case there is a nonzero intercept at Fr $= 0$, showing a minimum force is required to initiate motion in the bed, even in the absence of interparticle friction. The curve of force against Froude number follows a smooth form of $\bar{F}(\sqrt{\text{Fr}})$. The frictionless case has no tangential forces, and the drag force must therefore be dependent only on the geometry of the spherical intruder moving through the bed. No plateau in the force is found for Fr < 1 and no transition appears to exist at Fr $= 1$. This indicates that the approximately constant force found in the frictional cases for Fr < 1 is a consequence of both the intergranular frictional forces in addition to the geometrical effects of the spherical intruder moving through the bed.

The force on the intruder is transmitted through contacts with neighboring particles. It is therefore useful to consider a normalized local coordination number κ for the intruder. This is defined as the number of particles contacting the intruder n normalized by the average coordination number for all particles in the bed Z. This is multiplied by a nondimensionalized measure of relative surface area $(R + r)^2/(2\sqrt{3}r^2)$, where $2\sqrt{3}r^2$ is the area of a hexagon into which a particle in the bed would fit. A hexagonal area was chosen as the ideal kissing number for spheres in two dimensions is 6, and spheres were expected to pack approximately two dimensionally over the surface of the larger spherical intruder. Altogether, the quantity κ is given by

$$\kappa = \frac{Z}{n}\frac{(R+r)^2}{2\sqrt{3}r^2}. \quad (6)$$

The relationship between κ and Fr is plotted in Fig. 6 for all particles considered. The trend of this relationship is well fitted by $\kappa = 1 + \frac{1}{5}$Fr, which is plotted in Fig. 6 as a solid
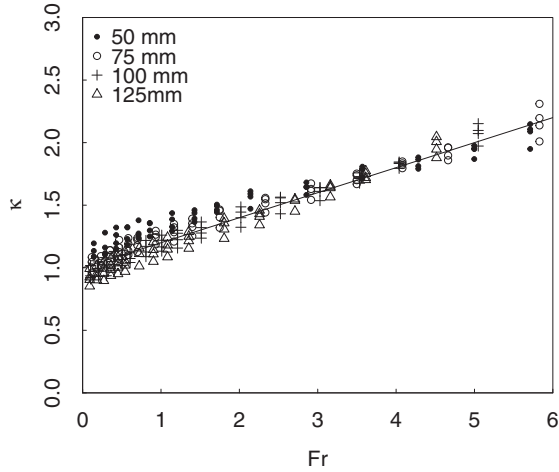
FIG. 6. Normalized contact number κ against Froude number for both frictionless particles and particles with friction angles 7.5°, 15°, and 30°. The solid line is a fit to the data of the form $\kappa = 1 + \frac{1}{5}\text{Fr}$.

black line. The interesting result that the intercept at Fr = 0 is close to 1 only holds if κ is defined using a hexagonal area. For the static case of Fr = 0, $n = Z(R + r)^2/(2\sqrt{3}r^2)$, providing an expression for the approximate number of contacts for an intruder in three dimensions, which is not easy to accurately determine [39].

The local contact number n also enables the expression of a linear relationship between the speed of the intruder and the resultant drag force. Figure 7 shows the function $F\sqrt{gR}/n$ plotted against the intruder speed v. This follows a linear form of

$$\frac{F\sqrt{gR}}{n} = \alpha + \beta v, \qquad (7)$$

where α and β are constants. In the limit $v \to 0$, $F/n = \alpha/\sqrt{gR}$, giving the minimum force per contact required to
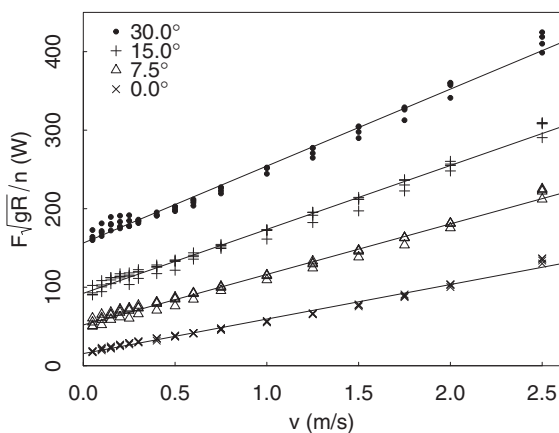

FIG. 7. Power dissipated per contact, $F\sqrt{gR}/n$, against imposed intruder speed v. The relationship is dependent on intergrain friction, but linear for all cases considered. The value at $v = 0$ gives the minimum power per contact which must be maintained to allow motion of the intruder within the bed α. The slope of the lines represents the constant effective frictional force per contact β. The zero friction case has both a nonzero intercept and slope, showing an effective frictional force in the absence of any intergrain friction.

mobilize the bed. Alternatively, the parameter α has units of power and can therefore be regarded as the minimum power per contact which must be maintained for structural rearrangements of the granular material to occur. The parameter β has units of force, and the product βv has units of power. As frictional power is dissipated as $\mu N v$, where μ is a friction coefficient and N is a normal force, we can equate this with the expression for βv to give $\mu \sim \beta/N$. From the definition of the friction coefficient $\mu = F_f/N$, where F_f is the frictional force, β can be identified as a per-contact dynamic frictional force resulting from the reorganization of the bed.

There is a nonzero intercept and slope in the case with zero friction. This shows that there is still an effective friction on the particle resulting purely from the rearrangement of particles within the bed. This effective friction acts even in the absence of interparticle friction. The parameters α and β in this case therefore represent a direct measure of the resistance to rearrangement of the granular material arising purely from the structural micromechanics within the bed. Interestingly, the existence of an effective friction for frictionless particles has previously been found, albeit in the context of a sheared cell [22] and biaxial compression of a granular material [20]. However, the effective friction observed here, resulting from localized rearrangements around an intruder, has not previously been reported.

IV. CONCLUSION

We have examined the drag forces on a spherical intruder particle immersed within a granular bed at low Froude number. Although the instantaneous forces on the intruder are highly variable, there is a well-defined mean force. For frictional systems, a linear dependence between force and Froude number was found for Fr > 1. For Fr < 1 the dependence between Force and Froude number is unclear but could be reasonably approximated as a constant force, which has previously been reported for systems in this regime. The observed dependence on Froude number can be explained in terms of the two characteristic time scales for the system $\tau_p \propto 2\sqrt{R/g}$ and $\tau_i \propto R/v$, with $\tau_p/\tau_i = \text{Fr}$. The case with no friction, in contrast, has no evident transition over the range of Froude numbers considered and has a smooth functional form $\bar{F}(\sqrt{\text{Fr}})$. This indicates that the approximately constant force observed for frictional granular material at very low intruder speeds is a purely frictional effect.

At higher Froude numbers, which were not considered in this study, a further transition to an inertial regime must exist. This inertial regime would be governed by a quadratic drag law, which can be seen by considering the force on a sphere impacted by a column of particles moving at a speed v. From dimensional considerations, this would be given by $F \sim \rho A v^2$, where A is the cross-sectional area of the intruder and ρ the bulk density of the bed. This quadratic dependence has, indeed, been reported in high-speed systems [30,31]. In this case, there appears to be three types of drag present in frictional granular systems: at very low Froude numbers, Fr < 1, the motion is quasistatic and there is an effectively constant force resulting from a limited bed rearrangement around the intruder. In this regime, particles do not lose contact with the intruder. At higher Froude numbers, Fr > 1, particles

lose contact with the rear of the intruder, causing a wake to form. Drag in this regime is governed by particles sliding over the forward face of the intruder, and appears linear with Froude number. Finally, at $Fr \gg 1$, inertial collisions dominate and the drag force follows a quadratic form.

The normalized contact number follows a linear trend of the form $\kappa = 1 + \frac{1}{5}Fr$ for both frictionless and frictional particles. Further work is required to investigate whether this trend holds in similar granular systems. Nevertheless, it is remarkable that a straightforward linear trend, which is independent of friction, can be found relating the dynamic properties of the bed Fr to the structural configuration around the intruder κ. We have also shown that the drag force per contact with the intruder follows a linear relationship of the form $F/n = \alpha/\sqrt{gR} + \beta Fr$. The parameter α is the power per contact required for structural rearrangements within the granular material. The parameter β is the dynamic drag force per contact in the bed. In the case of zero friction both α and β are nonzero, showing evidence for an effective granular friction resulting from only the local structural configuration of the bed.

This study highlights a number of important challenges for the multiscale characterization of granular drag. Foremost is the connection between the drag force and the underlying mesoscale mechanisms of confined force chain evolution and dilatancy. An interesting question is whether an expression for the resultant drag force per contact, under both frictionless and frictional conditions, can be derived from the micromechanics of the bed. This can be explored using structural analysis

of confined force chain buckling under quasistatic loading conditions [40]. The special case of zero friction in the static or quasistatic limit is particularly interesting from the standpoint of force chain evolution. As friction serves to stabilize the contacts, the absence of friction would leave geometrical interlocking as the only mechanism through which the material could mobilize resistance to a moving intruder. For a system comprising spherical particles, the degree of geometrical interlocking is small compared to that for assemblies of irregularly shaped particles. It would therefore be expected that the resultant force chains would be highly unstable for the cases with zero friction considered in this study. This is consistent with findings in an earlier study by Tordesillas *et al.* [13], which showed a relatively sparse force chain network develops beneath an indenting rigid punch in the low friction limit. Furthermore, a by-product of force chain buckling is the creation of voids between the buckling chain and the surrounding particles. In the large strain or so-called critical state regime in biaxial tests [21], systems with more stable force chains develop higher residual macroscopic void ratios due to their higher sliding friction and resistance to rotation. The next stage of this research is ongoing and is focused on unraveling these micromechanical details of granular drag. In particular, the evolution of the local contact topology and force chain network around the intruder will be characterized, as well as how this evolution is influenced by the competing driving forces of gravity and intruder motion.

[1] A. Drescher and G. de Josselin de Jong, J. Mech. Phys. Solids **20**, 337 (1972).

[2] F. Radjai, D. E. Wolf, M. Jean, and J.-J. Moreau, Phys. Rev. Lett. **80**, 61 (1998).

[3] T. S. Majmudar and R. P. Behringer, Nature (London) **435**, 1079 (2005).

[4] R. Arévalo, I. Zuriguel, and D. Maza, Phys. Rev. E **81**, 041302 (2010).

[5] A. Tordesillas, D. M. Walker, and Q. Lin, Phys. Rev. E **81**, 011302 (2010).

[6] A. Tordesillas, J. Zhang, and R. Behringer, Geomechanics and Geoengineering **4**, 3 (2009).

[7] J. Geng and R. P. Behringer, Phys. Rev. Lett. **93**, 238002 (2004).

[8] J. Geng and R. P. Behringer, Phys. Rev. E **71**, 011302 (2005).

[9] J. E. Hilton, P. W. Cleary, and A. Tordesillas, AIP Conf. Proc. **1542**, 843 (2013).

[10] I. Albert, J. G. Sample, A. J. Morss, S. Rajagopalan, A.-L. Barabási, and P. Schiffer, Phys. Rev. E **64**, 061303 (2001).

[11] J.-F. Métayer, D. J. S. III, C. Radin, H. L. Swinney, and M. Schröter, Europhys. Lett. **93**, 64003 (2011).

[12] J. Paavilainen and J. Tuhkuri, Cold Regions Science and Technology **81**, 1 (2012).

[13] M. Muthuswamy and A. Tordesillas, J. Stat. Mech.: Theory Exp. (2006) P09003.

[14] M. Small, D. M. Walker, A. Tordesillas, and C. K. Tse, Chaos **23**, 013113 (2013).

[15] L. Favier, D. Daudon, F. Donzé, and J. Mazars, J. Stat. Mech.: Theory Exp. (2009) P06012.

[16] T. Faug, P. Caccamo, and B. Chanut, Phys. Rev. E **84**, 051301 (2011).

[17] T. Faug, P. Caccamo, and B. Chanut, Geophys. Res. Lett. **39**, L23401 (2012).

[18] S. Moriguchi, R. Borja, A. Yashima, and K. Sawada, Acta Geotechnica **4**, 57 (2009).

[19] J. E. Hilton and P. W. Cleary, Phys. Rev. E **84**, 011307 (2011).

[20] N. Kruyt and L. Rothenburg, J. Stat. Mech.: Theory Exp. (2006) P07021.

[21] A. Tordesillas, Philosophical Magazine **87**, 4987 (2007).

[22] P.-E. Peyneau and J.-N. Roux, Phys. Rev. E **78**, 011307 (2008).

[23] K. Wieghardt, Mechanics Research Communications **1**, 3 (1974).

[24] R. Albert, M. A. Pfeifer, A.-L. Barabási, and P. Schiffer, Phys. Rev. Lett. **82**, 205 (1999).

[25] I. Albert, P. Tegzes, R. Albert, J. G. Sample, A. L. Barabási, T. Vicsek, B. Kahng, and P. Schiffer, Phys. Rev. E **64**, 031307 (2001).

[26] R. Soller and S. A. Koehler, Phys. Rev. E **74**, 021305 (2006).

[27] Y. Ding, N. Gravish, and D. I. Goldman, Phys. Rev. Lett. **106**, 028001 (2011).

[28] R. D. Maladen, Y. Ding, C. Li, and D. I. Goldman, Science **325**, 314 (2009).

[29] A. Levy and M. Sayed, Powder Technol. **181**, 137 (2008).

[30] F. Q. Potiguar and Y. Ding, Phys. Rev. E **88**, 012204 (2013).

[31] C. R. Wassgren, J. A. Cordova, R. Zenit, and A. Karion, Phys. Fluids **15**, 3318 (2003).

[32] J. F. Boudet and H. Kellay, Phys. Rev. Lett. **105**, 104501 (2010).

[33] M. P. Ciamarra, A. H. Lara, A. T. Lee, D. I. Goldman, I. Vishik, and H. L. Swinney, Phys. Rev. Lett. **92**, 194301 (2004).

[34] D. Chehata, R. Zenit, and C. R. Wassgren, Phys. Fluids **15**, 1622 (2003).

[35] Y. Tsuji, T. Tanaka, and T. Ishida, Powder Technol. **71**, 239 (1992).

[36] V. Šmilauer, E. Catalano, B. Chareyre, S. Dorofenko, J. Duriez, A. Gladky, J. Kozicki, C. Modenese, L. Scholtès, L. Sibille, J. Stránský, and K. Thoeni, in *Yade Documentation*, edited by V. Šmilauer, The Yade Project, 1st ed. (2010), http://yade-dem.org/doc/.

[37] B. Harthong, J. Jerier, P. Doremus, D. Imbault, and F. Donzé, Int. J. Solids Struct. **46**, 3357 (2009).

[38] C. Modenese, S. Utili, and G. T. Houlsby, in *Discrete Element Modelling of Particulate Media*, edited by C.-Y. Wu (Special Publication, Royal Society of Chemistry, 2012).

[39] A. R. Bausch, M. J. Bowick, A. Cacciuto, A. D. Dinsmore, M. F. Hsu, D. R. Nelson, M. G. Nikolaides, A. Travesset, and D. A. Weitz, Science **299**, 1716 (2003).

[40] A. Tordesillas and M. Muthuswamy, J. Mech. Phys. Solids **57**, 706 (2009).